JOURNAL OF SOLID STATE CHEMISTRY 41, 27–38 (1982)

Lanthanum β-Alumina Phase Doped with Europium: Optical Investigation by Dye Laser Site-Selective Excitation

J. DEXPERT-GHYS, M. FAUCHER, AND P. CARO

Laboratoire des Eléments de Transition dans les Solides CNRS, 1 Place A. Briandt, 92190 Meudon, France

Received July 30, 1981

Optical properties of Eu^{3+}-doped in (La) β-alumina are studied under conventional ultraviolet excitation and under site-selective excitation using a dye laser. The results are interpreted in terms of structural characteristics: eight different point sites are thus observed for Ln^{3+} (La^{3+} or Eu^{3+}). Following the spectroscopic as well as the previous X-ray diffraction analysis the mirror plane structure is described as the juxtaposition of microdomains in which Ln^{3+} ions have different immediate environments with 5 to 12 oxygen first neighbors.

Introduction

This work follows the results previously reported in the Ref. (*1*). In Ref. (*1*) we reported the crystallographic study of the lanthanum aluminate of approximate composition $11Al_2O_3/1La_2O_3$ hereafter noted (La) β-alumina and we studied the fluorescence properties of Eu^{3+} doped in this compound. In the present paper we return to the optical study by dye laser site-selective excitation. The optical results are interpreted in terms of local structural properties near Ln^{3+} and we try to establish an homogeneous model of the (La) β-Al structure in concordance with previous X-ray results.

The structure of (La) β-Al is closely related to those of the well-known (M^+) β-Al (M = Na, Ag, K, Tl) and of $BaAl_{12}O_{19}$ isomorphous of the magnetoplumbite $BaFe_{12}O_{19}$. All these compounds are characterized by spinel blocks (formula $(Al_{11}O_{16})^+$) separated by a mirror plane, in (or close to) which are located the bigger cations. The composition and the structure of this mirror plane differentiate the three structures. In the case of (M^+) β-Al, the ideal formula is $MAl_{11}O_{17}$ and the ideal mirror plane composition is then $[M^+O]^-$ but in fact all the (M^+) β-aluminas are nonstoichiometric and the real existence range does not contain the stoichiometric composition 11 Al_2O_3/M_2O but higher M_2O contents. The structure of these compounds has been extensively studied, for example, in Refs. (*2–15*). In the case of the magnetoplumbite structure the mirror plane formula is $[M'^{2+}Al0_3]^-$ and it is much more densely packed than in the β case. The problem of (La) β-Al structure also amounts essentially to the mirror plane structure as will be seen below.

I. Report of Previous Results Concerning (La) β-Al

The (La) β-Al phase was first identified

0022-4596/82/010027-12$02.00/0

by R. S. Roth *et al.* (*16*); for the compositions between 11 Al_2O_3/1 La_2O_3 (noted 11/1) and 12/1, they detected some irreproducible results in X-ray patterns. Other works on the systems Al_2O_3/Ln_2O_3 (Ln = La, Nd, Sm) (Refs. *17–20*) led approximately to the same conclusions, that is the existence of a β-type phase in a narrow composition range near 11/1. More recently A. L. N. Stevels *et al.* (*21*) established a rather different composition range for (La) β-Al extending from 13.07/1 to 13.89/1 and pointed out the magnetoplumbite character of this compound. On the contrary for R. C. Ropp *et al.* (*22*) the exact formula is 11/1 and the X-ray diffraction pattern for the 12/1 composition is different. For our part, following the microprobe analysis and structural considerations as exposed in Ref. (*1*), we suggest a range of compositions for (La) β-Al extending from 11/1 to about 14/1; it is remarkable that this range covers the values reported by those different authors.

In the present work we attempt to describe the structure which exists in nonstoichiometric (La) β-alumina. New experimental information was obtained by a more elaborate study of Eu^{3+} partially doped in the compound by dye laser site-selective excitation.

II. Experimental

The preparation of sintered samples, their analysis, their characterisation by X-ray diffraction and by fluorescence under ultraviolet excitation have already been reported in detail in Ref. (*1*). So we shall only describe the dye laser site-selective excitation of the europium fluorescence. The Eu^{3+} ion is often used as a structural microprobe. The information which can be deduced from the spectroscopic properties of this ion partially substituted for other Ln^{3+} has been described for example in Refs. (*23*) and (*24*). The Eu^{3+} fluorescence is mainly due to transitions $^5D_{J=0-3} \rightarrow {}^7F_{J=0-4}$ and can be measured at either 300, 77, or 4 K after excitation to upper levels under ultraviolet light. The fluorescence spectra exhibit characteristic features (number, relative intensities, and energetical positions of lines) which reflect the local structural properties nearby Eu^{3+}. If these active ions occupy several crystallographic sites in a given compound, all are excited simultaneously by the energetic (uv) incident light and the corresponding fluorescence spectra overlap; the individual spectra are then quite difficult to isolate. The technique of site-selective excitation allows to avoid this difficulty. It consists in exciting directly the $^7F_0 \rightarrow {}^5D_0$ transition of Eu^{3+} ions in a given site (each site is related to one $^7F_0 \rightarrow {}^5D_0$ energy value) and then analysing the particular $^5D_0 \rightarrow {}^7F_{J=1-4}$ fluorescent transitions of that site.

The experimental apparatus is made up of a Spectra Physics 375/376 jet stream dye laser pumped by a Spectra Physics 164 argon ion laser. The dye is Rhodamine 6G (10^{-3} M in ethyleneglycol). The wavelength of the laser beam is continuously tunable from about 5700 to 6500 Å, the linewidth being 0.7 cm^{-1}. All the fluorescence spectra are investigated with a Jarrel-Ash 78460 Czerny-Turner spectrometer (focal length 1 m). Conventional ultraviolet excitation is achieved by an Osram HBO 150-W lamp.

III. Results

(*a*) *X-Ray Diffraction*

The results of identification by X-ray diffraction, as well as the initial compositions and the notations used in the following are reported in Table I. The observed d_{hkl} agree rather well with those of Ref. (*22*) and in spite of some differences regarding intensities, the two series of results can probably be attributed to the same compound. Within the measurements precision (on

TABLE I

IDENTIFICATION OF THE DIFFERENT PHASES BY X-RAY DIFFRACTION AND FLUORESCENCE

Sample	Initial composition $m \cdot Al_2O_3/m' \cdot La_2O_3$	X-ray identified phases	Fluorescence identified phases
—	9.25/1	P($LaAlO_3$) + β	P
—	10.60/1	P + β	P + β (type β)
I	12.20/1	β	β (type β)
—	13.80/1	β + α (Al_2O_3)	Continuous evolution
II	16.90/1	β + α	↓
—	25.20/1	β + α	β (type magnetoplumbite)

powder samples) we detected no intensity modification due to composition variations.

The results of X-ray calculations as reported in Ref. (*1*) are (see Table II):

—the space group for (*Ln*) β-Al is $P6_3/mmc$ as for (M^+) β-Al and magnetoplumbite (1 *Ln* = 0.99 La + 0.01 Eu).

—the Ln^{3+} ions are located in the mirror plane.

—nearly all Ln^{3+} are located at the (2*d*) position or quite near it.

—the oxygen positions are (2*c*) or (6*h*) ($x = \frac{1}{8}$).

—(2*b*) is a cationic site. Following the composition, this position may be occupied either by Ln^{3+} and the mirror plane structure then resembles (M^+) β-Al, either by Al^{3+} (when aluminum content increases) and the mirror plane occupation is the same as in magnetoplumbite type phases.

The maximum number of lanthanum per unit cell is 2 and the theoretical limit composition towards high lanthanum contents is 11/1 ($[Al_{11}\ O_{16}]^+[LnO_2]^-$) (there are two mirror planes and two spinel blocks in one unit cell). For high aluminum contents the number of oxygen ions in (6*h*) ($x = \frac{1}{8}$) limits the mirror plane composition to $[M^{3+}_{5/3}\ O_3]^-$ ($M^{3+} = Ln^{3+} + Al^{3+}$) but the ratio between these cations cannot be fixed. If each unit cell is occupied by 2 Ln^{3+} the formula of one mirror plane is $[Ln_{3/3}\ Al_{2/3}\ O_3]^-$ (11.7/1). Following X-ray calculations it has been established that vacancies exist in the Ln^{3+} lattice, the resulting composition of the mirror plane may be, for exam-

TABLE II

RESULTS OF X-RAY INTENSITY REFINEMENT CALCULATIONS WITH RESPECT TO SITE OCCUPANCY IN THE MIRROR PLANE[a]

	2*d* ($\frac{2}{3}\ \frac{1}{3}\ \frac{1}{4}$)		2*b* (0 0 $\frac{1}{4}$)		6*h* (0.71 0.29 $\frac{1}{4}$)		2*c* ($\frac{1}{3}\ \frac{2}{3}\ \frac{1}{4}$)		6*h* ($\frac{1}{6}\ \frac{5}{6}\ \frac{1}{4}$)		
	ion	n^b	ion	n^b	ion	n^b	ion	n^b	ion	n^b	R^c
2	*Ln*	0.77	*Ln*	0.15	—	—	O	0.6	O	1.69	7.8%
3	*Ln*	0.77	Al	0.8	—	—	O	0.6	O	1.69	7.8%
4	*Ln*	0.37	*Ln*	0.16	*Ln*	0.39	O	0.59	O	1.44	7.5%
5	*Ln*	0.37	Al	0.85	*Ln*	0.39	O	0.58	O	1.44	7.5%

[a] These results were reported in Ref. (*1*).

[b] *n*: number of atoms per mirror plane and unit cell (one unit cell contains two mirror planes).

[c] $R = \Sigma|\ |F_o| - |F|\ |/\Sigma|F_o|$.

ple, $[Ln_{5/6} \square_{1/6} Al_{5/6} \square_{1/6} O_3]^-$ leading to the overall composition 14.2/1 which is not too far from the experimental microprobe determination and is built up with an equal number of Ln^{3+} and Al^{3+} in the mirror plane. This composition is likely to represent a β phase with high aluminum contents. So, by varying the nature and number of ions in ($2b$), one can account for the observed composition range.

An important point to note is that several kinds of oxygen positions have to be occupied in order to ensure the electrical neutrality. The real situation $[M_x^{3+} O_{(3x+1)/2}]^-$ is intermediate between a total ($2c$) occupancy which would lead to $[M^{3+} O]^+$ and a total ($6h$) occupancy which would lead to $[M_{5/3}^{3+} O_3]^-$. As a consequence of this partial occupancy, several immediate neighborings are associated with each of the two cationic positions and two Ln^{3+} ions may occupy the same crystallographic position and nevertheless have different local symmetry. The different possible point sites are schematized in Fig. 1 and are either D_{3h} (Figs. 1A, B, C, and G), or Cs (Figs. 1D, E, and F).

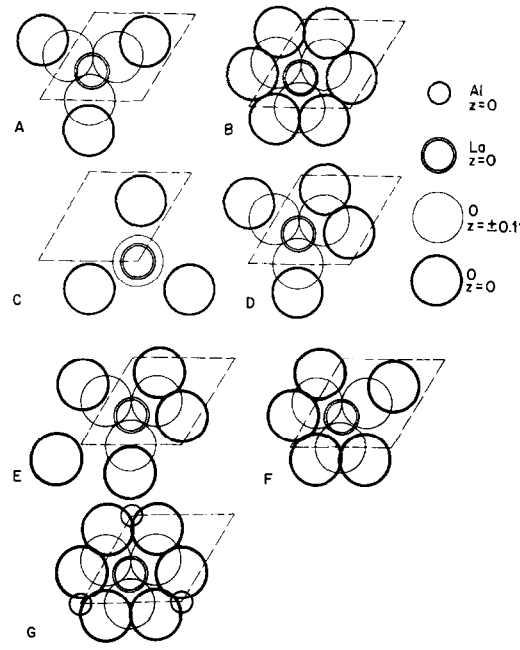

FIG. 1. Different point sites for Ln^{3+}: projection on (001).

(b) Fluorescence under Ultraviolet Excitation

As was shown in Ref. (*1*), the aspect of fluorescence spectra of Eu^{3+} in (La) β-Al varies considerably and in a progressive way with the initial composition. In Fig. 2 are shown the fluorescence spectra recorded at 77 and 300 K for samples I and II (compositions are given in Table I). Each spectrum is complex and is due to Eu^{3+} in more than one site. For a given temperature, some lines are common to the two spectra but their relative intensities are changed with the composition. The aim of the present work is to find the structural hypothesis which explains these modifications in a coherent way with diffraction data.

For a given composition, the relative fluorescence intensities also vary with the temperature, we shall try to give an explanation for this phenomenon later (Section III.e).

(c) Fluorescence under Laser Excitation

We have analysed the fluorescence of Eu^{3+} under site-selective excitation for the two samples I and II (cf, Table I). These two samples were chosen because they present spectra characteristic of high lanthanum contents for I (mean composition 12.2/1) and of high aluminum contents for II (approximate composition 14.7/1) and they cover the real composition range of (La) β-Al. The lines of the $^5D_0 \rightarrow {}^7F_0$ transition were located under uv excitation and then the laser excitation wavelength λ_e was fixed successively on each of them and the corresponding fluorescence spectrum was recorded. When two or several spectra appeared simultaneously we tried to enhance each of them successively by slightly modi-

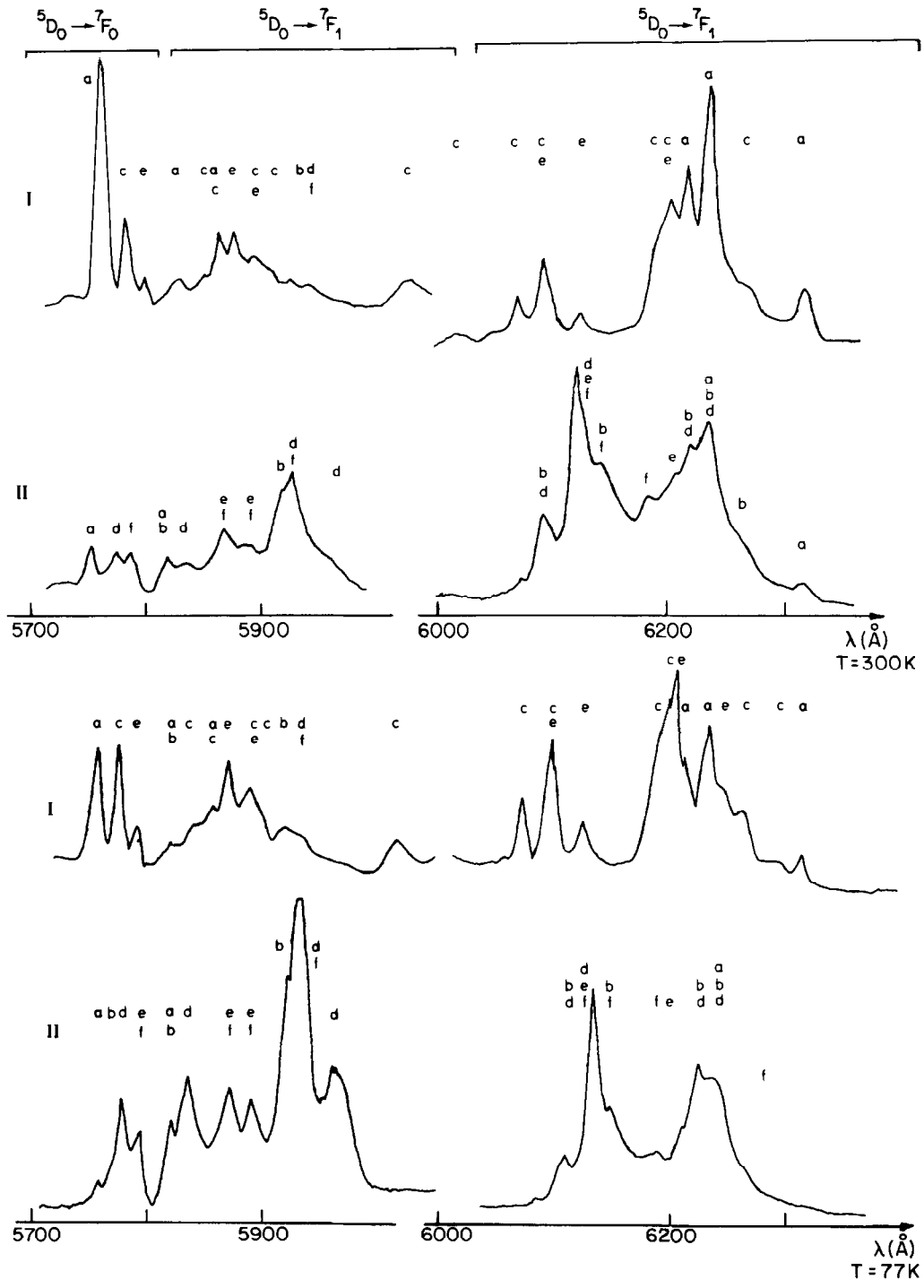

FIG. 2. Fluorescence spectra of Eu^{3+} in (La) β-Al under ultraviolet excitation (at 77 and 300 K).

fying λ_e. These results are reported on Table III and Fig. 3, we have labeled the different spectra *a*, *b*, *c*, etc. Three basically different kinds of spectra are thus identified.

(1) Type *a*, isolated for both I and II samples, is quite different from the others mainly for the $^5D_0 \rightarrow {}^7F_2$ transition. For this spectrum three $^5D_0 \rightarrow {}^7F_1$ lines are identified. Their barycenter at 435 cm^{-1} above $^7F_0$ is very high, but this value agrees well with the other experimental data which

TABLE III

SITE-SELECTIVE EXCITATION: NUMERICAL RESULTS

	$^5D_0 \rightarrow {}^7F_0$	$^5D_0 \rightarrow {}^7F_1$			$^5D_0 \rightarrow {}^7F_2$			
Notation	λ_e (Å)	λ (Å)	$^7F_1$ levels (cm^{-1})	Barycenter	λ (Å)	$^7F_2$ levels (cm^{-1})	Barycenter	Sample
a	5749	5817	203		6055	879		
		5854	312	435	6085	960		I
		6022.5	790		6212.5	1297	1207	
					6232.5	1349		(II)
					6312.5	1552		
b	5762.5	5815	157		6090	934		
		5915	448	408	6113	995		II
		5975	618		6132.5	1047	1117	
					6225	1290		I
					6237	1321		
c_1	5770	5840	208		6058	824		
		5859	263	400	6072	862		I
		5880	324	(see text)	6187	1168		(II)
		6010	692		6262	1362		
c_2	5773	5844	206		6094	912		
		5876	304	410	6110	955		I
		5885	359	(see text)	6195	1180		(II)
		6010	683		6298	1444		
d	5774	5834	178		6100	926		
		5929	453	392	6124	990		II
		5962	546		6195	1177	1119	
					6216	1232		(I)
					6230	1268		
e	5786	5862	224		6093	871		
		5885	291	414	6098	884		I
		6040	727		6125	957	1032	
					6204	1164		(II)
					6250	1283		
f_1	5789.5	5870	237		6152	1018		
		5888	289		6170	1066		II
					6260	1299		
f_2	5791	5925	390		6121	931		
					6145	995		II
					6175	1074		
					6245	1255		

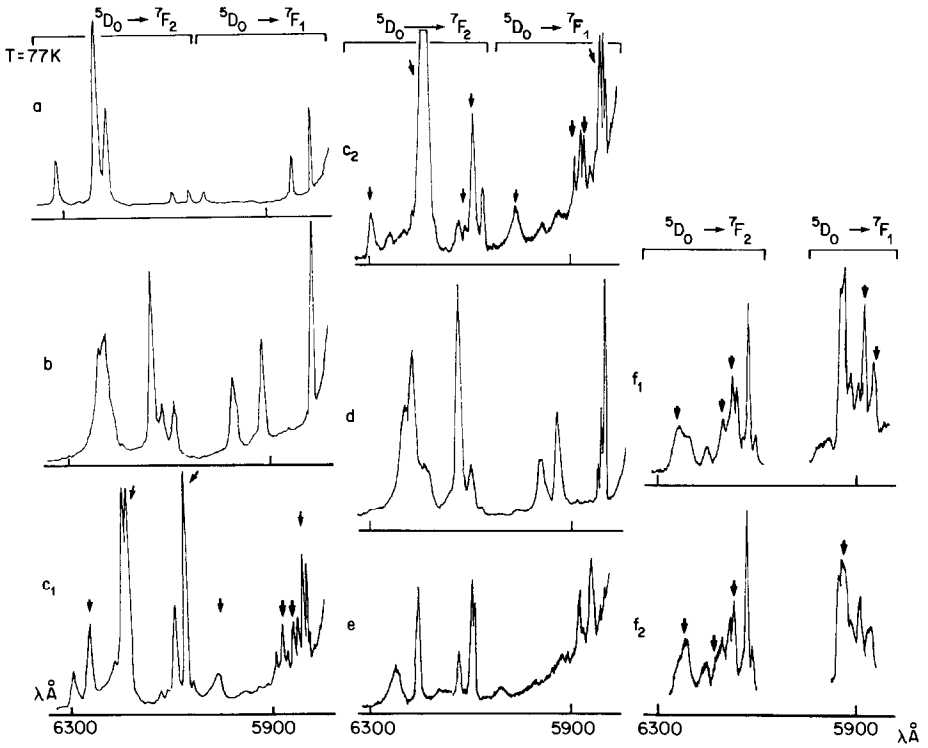

FIG. 3. Fluorescence under site-selective excitation for samples I and II (arrows correspond to the site directly excited).

are given in Fig. 4 (following the Refs. *(25, 32)*.

(2) *b*, c_1, c_2, *d*, *e*, present similar characteristics and have been observed in the two samples. c_1, c_2, and *d* appear for very close λ_e values and are then quite difficult to isolate mainly in the $^5D_0 \rightarrow {}^7F_1$ transition, where there remain some ambiguities. In particular, for $\lambda_e = 5770$ and 5773 Å, $c_1 + c_2$ appear; but in each case some lines are enhanced (indicated by arrows in the Fig. 4) and are then attributed to the corresponding $\lambda_e = {}^5D_0 \rightleftarrows {}^7F_0$. The fact that two or more spectra appear simultaneously may be attributed to simultaneous excitation within the width of the exciting laser beam. The energy transfer between Eu^{3+} ions at different sites is highly improbable in (*Ln*) β-Al at such doping levels (1Eu/100*Ln*). The mean Eu–Eu distance may be estimated to 30 Å (unit cell volume = 576 $Å^3$ for 0.02 Eu^{3+} atoms), this distance is sufficient to inhibit energy transfer between two rare earth ions (and in fact transfer from the highly energetic *a* $^5D_0$ is not observed).

(3) f_1 and f_2 are observed only with sample II and are hardly separated from another, and also from *e*. Those two spectra are difficult to excite, probably due to the weakness of the $^7F_0 \rightarrow {}^5D_0$ absorption transition.

(*d*) *Number and Relative Abundance of the Different Sites*

Each particular spectra corresponds to a particular neighborhood around the active ion. For the high lanthanum content sample I we have thus isolated six different spectra corresponding to six different surroundings for Ln^{3+}. But among those *a*, *b*, c_1, c_2, and *e* suffice to form the global spectrum obtained under uv excitation. *d* was observed in

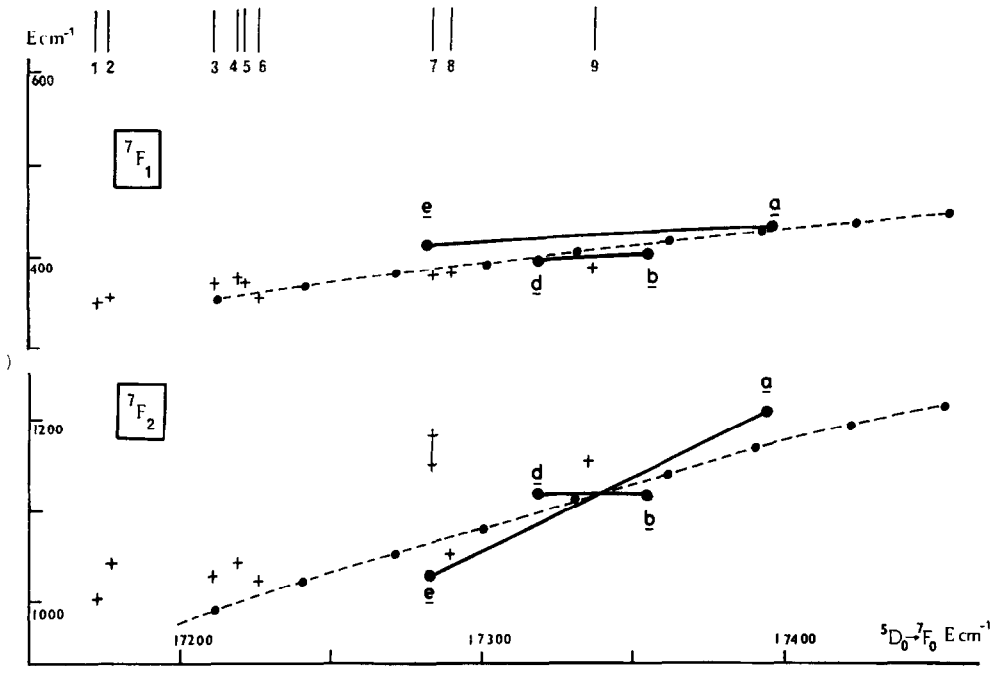

FIG. 4. $^7F_1$ and $^7F_2$ Eu^{3+} barycenters positions versus $^5D_0 \rightarrow {}^7F_0$ energy. 1 and 2: B-Gd_2O_3 (spectra B and C) (Ref. (*25*)); 3: YPO_4 (Ref. (*26*)); 4: A-La_2O_3 (Ref. (*27*)); 5: C-Y_2O_3 (Ref. (*28*)); 6: $LaAlO_3$ (Ref. (*29*)); 7: B-Gd_2O_3 (spectrum A) (Ref. (*25*)); 8: Eu P_5O_{14} (Ref. (*30*)); 9: $3Y_2O_3/WO_3$ (Ref. (*31*)); 10: sodium–baryum–zinc silicate glass (Ref. (*32*)).

sample I by laser excitation because this technique is very effective when there is an exact resonance between λ_e and $^7F_0 \rightarrow {}^5D_0$, even if the corresponding site appears only as an "impurity" in the sample. In the same way the high-aluminum-content sample II exhibits *b*, *d*, *e*, f_1, and f_2 spectra. For this sample *a*, c_1, and c_2 are "impurity sites."

At this stage it is important to point out that *a* is characteristic of high lanthanum content (sample I, of β-type), whereas f_1 and f_2 are characteristic of high aluminum contents (sample II, of magnetoplumbite type).

(*e*) *The Effect of Temperature*

The structural analysis was performed at 300 K and the optical investigations reported hereabove at 77 K; but as already pointed out (III.b), the global spectra exhibit modifications between 77 and 300 K; so, in order to check the influence of temperature, X-ray patterns on samples I and II were recorded at 77 K.

Low-temperature X-ray diffraction measurements were obtained by B. Chevalier (University of Bordeaux I, France) on the experimental apparatus described in Ref. (*33*). For each sample the patterns were identical at 77 and 300 K, this indicates that no drastic structural modification such as a phase transition occurs between those two temperatures.

For the fluorescence spectra, the same positions for the lines are observed at both temperatures, but at 300 K the total intensity emitted in the visible range is smaller and the lines of site *a* are greatly enhanced with respect to the lines of the other sites. There is no evidence for *a* to be a vibronic spectrum. One could explain the relative enhancement of *a* by a rearrangement of ox-

ygen in the mirror plane, so as to create more and more *a* optically active sites as the temperature rises, by a reversible process. In fact it is difficult to evaluate the relative proportion of different sites by fluorescence experiments on doped materials since a large number of factors, besides concentration, can affect the observed intensities, i.e., feeding of the $^5D_0$ level, efficiency of nonradiative processes, etc. In what concerns quantitative estimation, more trust must be put in X-ray analysis.

(f) Nature of the Sites

As was established in Section IIIa, the point symmetry at Ln^{3+} site is either C_s or D_{3h}. The number of lines allowed by group theory for $^5D_0 \rightarrow {}^7F_0$, $^7F_1$, $^7F_2$ transitions is (1, 3, 5) in the first symmetry and (0, 2, 1) in the second. Most of the spectra isolated by site selective excitation exhibit three lines for $^5D_0 \rightarrow {}^7F_1$ and 4 or 5 lines for $^5D_0 \rightarrow {}^7F_2$ and may then be attributed to Eu^{3+} in a low C_s symmetry. In fact the *a* spectrum may be considered as resulting from Eu^{3+} in a slightly distorted D_{3h} site. It may be described in the following way: one doublet and one singlet for $^5D_0 \rightarrow {}^7F_1$, two doublets and one singlet for $^5D_0 \rightarrow {}^7F_2$. This disposition agrees with the decomposition under D_{3h} of levels $J = 1$ (A_2' singlet E'' doublet) and $J = 2$ (A_1' singlet + E' doublet + E'' doublet). We may now try to establish which of the three D_{3h} point sites (Fig. 1A, B, or C) is responsible for *a*; This is done:

(1) by evaluating the experimental crystal field parameters B_0^2.

(2) by calculating B_q^4 using the a priori point charge electrostatic model (PCEM) for each A, B, C case, and determining what structural hypothesis agrees best with the experimental $^7F_2$ disposition. These methods have already been described elsewhere (Refs. (*24, 25*)) and we shall give only the results here.

The position of the isolated $^7F_1$ line at 335 cm^{-1} above the barycenter leads in first approximation to $B_0^2 = +1780$ cm^{-1}. B_2^2 is weak and is fixed at zero as in true D_{3h} symmetry. The corrected B_q^4 values calculated a priori considering only the Ln^{3+} first neighbors (see Ref. (*25*)) are reported in Table IV together with the calculated energy levels for $^7F_2$ obtained by resolving the ^7F interaction matrix (see Ref. (*23, 24*)). The two structural hypotheses—Fig. 1A (coordination number $CN = 9$) and Fig. 1B ($CN = 12$)—lead to a correct disposition for $^7F_2$, that is the singlet line A_1' displaced toward high energies. Although the a priori calculations do not fit the observed spectrum exactly they permit to show that *a* is actually consistent with Eu^{3+} in one of the presupposed local environments of more or less distorted D_{3h} symmetry. This distortion cannot be estimated but it allows the appearance of lines forbidden in the true D_{3h} symmetry. Note that the other D_{3h} environment (Fig. 1G) has not been considered because it is characteristic of high aluminum contents (magnetoplumbite type environment, see IIIa), composition for which the *a* spectrum does not appear under conventional excitation.

(g) Fluorescence Linewidths

The observed linewidths under uv and site-selective excitation are of the same order (that is about 20 cm^{-1} at 77K). These values are higher than in well ordered oxides [that is about 10 cm^{-1} for Eu^{3+} in B-Gd_2O_3 measured with the same experimental apparatus (*24*)]. On the contrary, in glassy matrices the inhomogeneous linewidth under uv excitation is typically more than 100 cm^{-1} (*32*). So we have not to consider, as was done for silicate glasses, a progressive modification of the coordination around Ln^{3+} leading to an infinity of slightly different point sites. But rather the structure of (La) β-Al has to be considered as made of a relatively high but limited number of very different local environ-

TABLE IV

CALCULATED $^7F_2$ SUBLEVELS ENERGIES ΔE (WITH RESPECT TO THE BARYCENTER) IN THREE DIFFERENT LOCAL ENVIRONMENTS

Site 1A (CN = 9)[a]		Site 1B (CN = 12)[a]		Site 1C (CN = 5)[a]	
B_q^k (cm^{-1})	ΔE (cm^{-1})	B_q^k (cm^{-1})	ΔE (cm^{-1})	B_q^k (cm^{-1})	ΔE (cm^{-1})
B_0^2 = +1780[b]		B_0^2 = +1780		B_0^2 = +1780	
	E' = −224		E' = −251		E' = −332
B_0^4 = −96[c]		B_0^4 = +449		B_0^4 = +1722	
	E'' = +67		E'' = +114		A_1' = +182
B_0^6 = −216		B_0^6 = −348		B_0^6 = +559	
	A_1' = +312		A_1' = +274		E'' = +239
B_6^6 = −52		B_6^6 = +236		B_6^6 = −46	

[a] The experimental disposition: $E' \sim -288$ cm^{-1}, $E'' \sim +116$ cm^{-1}, $A_1' \sim +345$ cm^{-1} corresponds to either 1A or 1B.

[b] B_2^0 is the experimental value.

[c] B_q^4 and B_q^6 are calculated as in Ref. (*25*).

ments for Ln^{3+}. This is consistent with a description in terms of microdomains.

IV. Discussion and Structural Model

The properties (X-ray diffraction and optical spectra) studied on samples I and II cover the whole range of existence of β-alumina. As was suggested in (*1*), the fact that X-ray diffraction patterns remain unchanged when varying the composition leads us to reject the hypothesis of several different compounds and to support the existence of a composition range which lies between 11 Al_2O_3/1 La_2O_3 (formula $[Al_{11}O_{16}]^+[LaO_2]^-$) and approximately 14.2 Al_2O_3/1 La_2O_3 (formula $[Al_{11}O_{16}]^+[La_{5/6}Al_{5/6}O_3]^-$) (cf. Section IIIa).

The conclusions of the present spectroscopic study by site selective excitation of Eu^{3+} partially substituted for La^{3+} may be summarized in the following way:

—there are at least eight different immediate surroundings for Ln^{3+} in the composition range.

—Six of them are seen for all compositions but their relative proportion depends strongly on composition. One of the spectra (*a*) may be described in a semiquantitative way as resulting from a distorted D_{3h} site.

—The high Al^{3+} contents are characterized by the same six ones plus two more spectra (f_1 and f_2).

—each Ln^{3+} site is well defined and exhibits rather narrow fluorescence lines; energy transfer from site to site does not occur.

These experimental results are consistent with the description of the (La) β-Al structure as an ordered skeleton of spinel blocks $[Al_{11}O_{16}]^+$ separated by a mirror plane whose nature and structure vary with the overall composition. The (M^+) β-aluminas have already been described in a similar way, in terms of more or less extended microdomains in the mirror plane (*2, 3, 5*); but in the case of (La^{3+}) β-Al the nonstoichiometry always appears as a lack of La^{3+} (or excess of Al^{3+}) with respect to the composition 11 Al_2O_3/1 Ln_2O_3 so the mirror plane structure is rather like in the magnetoplumbite structure.

We tried to build a structural model in agreement with the experimental data in which the Ln^{3+} point sites are those of Figs. 1A–G.

For high lanthanum content; i.e., a mirror plane structure corresponding to $[LnO_2]^-$, Fig. 5a is an acceptable cell, where the electrical neutrality is attained for four $[Al_{11}O_{16}]^+$ units. It is possible to build other cells with 8, 12, . . . units, and the same overall composition. The remarkable point is that if the same rule is observed; i.e., there are no vacancies in the lanthanum framework, the mean composition in term of crystallographic positions will always be the same, that is:

$$[Ln(2d \text{ or } 6h)O(2c)_{0.5}O(6h)_{1.5}]^-.$$

Moreover if we make the reasonable postulate that the lanthanum ions which experience a nonsymmetrical environment (due to first neighbors) will be displaced in ($6h$) positions, we obtain a still more precise composition of the mirror plane:

$$[Ln(2d)_{0.5}Ln(6h)_{0.5} O(2c)_{0.5}O(6h)_{1.5}]^-. \quad (1)$$

This arrangement corresponds to a total cationic occupancy factor of 1 (over ($2d$) and ($6h$) sites) and if it were repeated throughout the crystal, the overall composition of (La) β-Al would be 11/1.

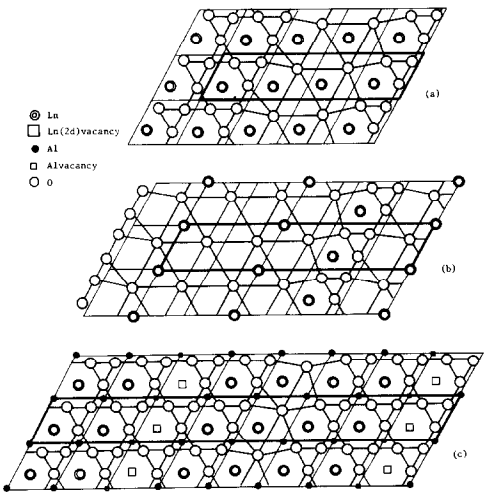

FIG. 5. Structural model for the mirror plane in (La) β-Al. The heavy lines delimit the cells used in the description of section IV; normal lines schematize the oxygen coordination around the cations; lighter lines delimit the (La) β-Al unit cell.

But the X-ray diffraction (Table II) strongly suggests an incomplete occupancy of sites $2d$ (or $6h$), and a partial occupancy of ($2b$). In fact, the presence of Ln^{3+} in ($2b$) leads rapidly to a deficiency in oxygen since anionic ($6h$) positions cannot be simultaneously occupied because of steric hindrance, therefore we have to admit the coexistence of Ln ($2b$) with Ln ($2d$ or $6h$) in another type of cell which could be that represented Fig. 5b the formula of which averaged over one $[Al_{11}O_{16}]^+$ unit is:

$$[Ln(6h)_{0.2}Ln(2b)_{0.4}O(2c)_{0.8}O(6h)_{0.6}]^-. \quad (2)$$

The simultaneous presence of cells (1) and (2) in the proportion of 3/1 would lead to the composition.

$$[Ln(2d)_{0.375}Ln(6h)_{0.425}Ln(2b)_{0.1} O(2c)_{0.575}O(6h)_{1.275}]^-$$

The agreement with calculation 4 of Table II is rather good.

The same line of argument can be followed for aluminum-rich compounds. The overall composition of the cell represented in Fig. 5c is approximately that given by the X-ray calculations 3 or 5 of Table II. In the same way as above, a more precise composition in term of crystallographic positions can be predicted by inspection of Fig. 5c as:

$$[Ln(2d)_{0.5}Ln(6h)_{0.25}Al(2b)_{0.75} O(2c)_{0.125}O(6h)_{2.625}]^-.$$

We approach from calculation 3 of Table II, where all the lanthanum atoms are in symmetrical positions ($2d$). The amount of O($6h$) has increased appreciably without attaining the desired value, but it is noteworthy that the trend is observed.

We propose here a homogeneous scheme to illustrate the two boundary compositions but none of the unit cells hereabove described is sufficient to account for the real samples (additional diffraction lines would

then be observed). The real mirror plane structure is probably a juxtaposition of microdomains corresponding to these different hypotheses, which explains the relatively narrow fluorescence lines observed. We can estimate grossly the magnitude of a microdomain by comparing the linewidths of the $^5D_0 \rightarrow {}^7F_1$ transition of Eu^{3+} in well ordered oxides and in (La) β-Al. The extra linewidth (10 cm^{-1}) in the latter can be attributed to the scattering of B_q^2 values due to disorder in the lattice (boundaries between different microdomains in our hypothesis). We can crudely write $\Delta E \simeq 0.2\Delta B_2^0$, which leads to $\Delta B_2^0 \simeq 50\ cm^{-1}$). This fluctuation is still typically observed around 40 Å when one computes B_2^0 by the point charge model within shells of increasing radii. We can therefore estimate the magnitude of reproducible domains to be more or less equal to 40 Å, which represents 7 (La) β-Al unit cells or two cells such as the one represented Fig. 5a. From this crude argument we can estimate the smallest microdomain to be a repetition of four cells such as the one represented Fig. 5a.

Acknowledgments

The authors wish to thank Dr. S. A. Brawer for very helpful discussions and Dr. B. Chevalier for the low-temperature X-ray diffraction experiments.

References

1. J. DEXPERT-GHYS, M. FAUCHER, AND P. CARO, *J. Solid State Chem.* **19,** 193 (1976).
2. C. R. PETERS, M. BETTMAN, J. W. MOORE, AND M. D. GLICK, *Acta Crystallogr. Sect. B* **27,** 1826 (1971).
3. W. L. ROTH, *J. Solid State Chem.* **4,** 60 (1972).
4. P. D. DERNIER AND J. P. REMEIKA, *J. Solid State Chem.* **17,** 245 (1976).
5. J. P. BOILOT, P. COLOMBAN, G. COLLIN, AND R. COMES, *Solid State Ionics* **1,** 69 (1980).
6. D. GOURIER, D. VIVIEN, AND J. LIVAGE, *Phys. Status Solidi A* **56,** 247 (1979).
7. Y. LE CARS, R. COMES, L. DESCHAMPS, AND J. THERY, *Acta Crystallogr. Sect. A* **30,** 305 (1974).
8. J. K. AKRIDGE AND J. H. KENNEDY, *J. Solid State Chem.* **29,** 63 (1979).
9. L. C. DE JONGHE, *J. Mater. Sci.* **12,** 497 (1977).
10. H. SATO AND Y. HIROTSU, *Mater. Res. Bull.* **11,** 1307 (1976).
11. J. O. BOVIN AND M. O'KEEFE, *J. Solid State Chem.* **33,** 37 (1980).
12. W. HAYES AND L. HOLDEN, *J. Phys. Colloq.* **13,** L321 (1980).
13. R. C. BARKLIE, J. R. NIKLAS, AND J. M. SPAETH, *J. Phys. Colloq.* **13,** 1757 (1980).
14. J. B. BATES, T. KANEDA, J. C. WANG, AND H. ENGSTROM, *J. Chem. Phys.* **73,** 4 (1980).
15. T. KODAMA AND G. MUTO, *J. Solid State Chem.* **17,** 61 (1976).
16. R. S. ROTH AND S. HASKO, *J. Amer. Ceram. Soc.* **41**(4), 146 (1958).
17. M. ROLIN AND P. H. THANH, *Rev. Int. Hautes Temp. Refract.* **2,** 175 (1965).
18. D. GOLDBERG, *Rev. Int. Hautes Temp. Refract.* **5,** 181 (1968).
19. E. T. FRITSCHE AND L. G. TENSMEYER, *J. Amer. Ceram. Soc.* **50**(3), 167 (1967).
20. I. A. BONDAR AND M. A. TOROPOV, *Izv. Akad. Nauk. SSSR, Ser. Khim.* **2,** 212 (1966).
21. A. L. N. STEVELS AND A. D. M. SCHRAMA DE PAUW, *J. Lumin.* **14,** 147 (1976).
22. R. C. ROPP AND G. G. LIBOWITZ, *J. Amer. Ceram. Soc.* **61,** 11 (1978).
23. P. CARO, "Structure électronique des eléments de transition." Presses Univ. France, Paris (1976).
24. J. DEXPERT-GHYS, Thèse de Doctorat d'Etat, Orsay (October 1979).
25. J. DEXPERT-GHYS, M. FAUCHER, AND P. CARO, *Phys. Rev. B* **23,** 2 (1981).
26. C. LINARES, A. LOUAT, AND M. BLANCHARD, *Struct. Bonding* **33,** 179 (1977).
27. C. LINARES AND F. GAUME-MAHN, *C. R. Acad. Sci. Paris Ser. B* **277,** 431 (1973).
28. J. DEXPERT-GHYS AND M. FAUCHER, *Phys. Rev. B* **20,** 1 (1979).
29. M. FAUCHER AND P. CARO, *J. Chem. Phys.* **63,** 1, 446 (1975).
30. C. BRECHER, *J. Chem. Phys.* **61**(6), 2297 (1974).
31. O. BEAURY, M. FAUCHER, AND P. CARO, *Mater. Res. Bull.* **13,** 175 (1978).
32. C. BRECHER AND L. A. RISEBERG, *Phys. Rev. B* **13,** 1 (1976).
33. J. ETOURNEAU, B. CHEVALIER, AND L. RABARDEL, *J. Phys. E* **8,** 930 (1975).